Fatigue-induced grain growth and formation of slip bands in Cu processed by equal channel angular pressing

M. Goto[1], M. Baba[1], S. Z. Han[2], J. Kitamura[1], T. Yamamoto[1], J.-H. Ahn[2], T. Yakushiji[3], S. Kim[4] & J. Lee[5]
[1]*Department of Mechanical Engineering, Oita University, Japan*
[2]*Korea Institute of Materials Science, Republic of Korea*
[3]*National Institute of Technology, Oita College, Japan*
[4]*Gyeongsang National University, Republic of Korea*
[5]*Changwon National University, Republic of Korea*

Abstract

In order to elucidate the effect of the microstructure on fatigue behavior of ultrafine grained copper, fatigue tests were conducted using copper processed by equal channel angular pressing through 4, 8 and 12 pass numbers. The evolution of microstructure and surface damage during cyclic stressing was monitored. For samples processed by 8 and 12 passes, dynamically recrystallized grains were formed and these grew with subsequent stressing. Slip bands were initiated inside such grains. For samples processed by 4 passes, the formation of slip bands was likely to occur inside dynamically recovered coarse grains. The physical basis on the phenomena leading to the initiation of fatigue cracks was discussed from the viewpoint of microstructure and surface damage evolution.
Keywords: fatigue, ultrafine grain, copper, slip bands, grain coarsening.

1 Introduction

Recently, a technique of processing of ultrafine grain (UFG) metals and alloys, based on severe plastic deformation (SPD) has been developed. One of the most common SPD methods for producing bulk UFG materials with grain sizes ranging from ~0.1 to 1 μm is the equal channel angular pressing (ECAP) technique [1].

WIT Transactions on Modelling and Simulation, Vol 59, © 2015 WIT Press
www.witpress.com, ISSN 1743-355X (on-line)
doi:10.2495/CMEM150251

For the envisaged structural applications, the fatigue characteristics of UFG materials have been studied with a particular focus on S–N plots, formation of shear bands and underlying microstructural mechanisms [2–7]. Regarding slip band formation in conventional grain-sized materials, the larger the grain sizes are, the smaller the slip resistance is. Therefore, the resistance to generation of decisive localized damage which cause the stress concentration required for fatigue crack initiation is reduced in the coarse grains. It has been shown that coarse grains are formed in the post-fatigued UFG copper as a result of dynamic recrystallization [5, 8, 9]. This indicates that the coarse grains in UFG copper should become the initiation site of fatigue cracks, because that fatigue cracks are generally initiated on the specimen surface at sites of severe cyclic strain localization. On the other hand, since the physical and mechanical responses of materials and alloys are significantly affected by the microstructure, e.g., the dependence of the yield stress (YS) on the grain size is well described by the Hall–Petch relationship, grain refinement achievable by SPD techniques has been of particular interest over the past few decades. The UFG microstructure processed by ECAP is sensitive to the parameters of the procedure, such as route, number of passes, deformation rate, shape of the die and temperature [10]. In order to elucidate the effect of the microstructure on fatigue strength of UFG materials, the change in morphological features of surface damage as a result of cyclic stressing should be monitored. However, such studies are few and certain questions remain unanswered.

In the present study, fatigue tests of copper (99.99% Cu) processed by ECAP through 4, 8 and 12 passages were carried out under the same test conditions. The effect of number of passes on the phenomena leading to the initiation of fatigue cracks was discussed from the viewpoint of microstructure and evolution of surface damage as a result of cyclic stressing.

2 Experimental procedures

The material used was pure oxygen-free copper (99.99 wt% Cu). Before ECAP processing, the materials were annealed at 500°C for 1 h (grain size, 100 μm). The ECAP die had a 90° angle between intersecting channels. The angles at the inner and outer corners of the channel intersection were $\Phi = 90°$ and $\Psi = 45°$, respectively. For this die geometry with a 45° outer corner, the plastic strains were not confined within the plane of intersection between two channels as is assumed in ECAP by simple shear (the deformation zone in the present die has a fan shape), giving rise to inhomogeneity of plastic strain in the channels. However, the effect of the die shape on the experimental results appeared to be negligible as was discussed in a previous work [11]. Repetitive ECAP was following route Bc (after each pressing, the billet bar was rotated 90° in the same sense around its longitudinal axis). The ECAP processing was conducted at a room temperature. MoS_2 was used as a lubricant for each pressing, and the pressing speed was 5 mm/sec. The number of ECAP passes used in this study was 4, 8 and 12, and hereafter samples are referred to as UFG 4, 8 and 12, respectively. Using the investigation of Iwahashi *et al.* [12] it was determined that the equivalent strain, ε, was 3.9, 7.8 and 11.7 for UFG4, 8 and 12, respectively.

The tensile test specimens were cylindrical, 4 mm in diameter and 40 mm long. The tensile tests were conducted on all the specimens at room temperature on an Instron-4208 testing machine at a strain rate of 1.6×10^{-3} s^{-1}. Round-bar fatigue specimens, 5 mm in diameter, were machined from their respective processed bars. Although the specimens had shallow circumferential notches (20 mm notch radius and 0.25 mm notch depth), the fatigue strength reduction factor for this geometry was close to 1, meaning that specimens could be considered plain. In order to remove any surface layer affected by the machining, the specimen surfaces were polished electrolytically approximately ≈25 μm from the surface layer prior to fatigue testing.

All fatigue tests were performed at room temperature using a rotating-bending (R-B) fatigue machine of constant bending-moment type operating at 50 Hz. The fatigue damage on the specimen surface was observed using an optical microscope (OM) and a scanning electron microscope (SEM). The stress value used was the nominal stress amplitude, σ_a, at the minimum cross-section (5 mm diameter).

The distribution of the grain sizes and GB misorientation were determined by electron backscatter diffraction (EBSD) analysis. The specimens were ground using silicon carbide paper and polished with polycrystalline 3 and 1 μm diamond suspensions. Final polishing was performed using a 0.04 μm colloidal silica suspension for 30–60 min. EBSD mapping was executed using a Tescan Mira II SEM incorporating an EDAX-TSL Hikari EBSD detector. Each hexagonal pixel was 40 nm for the UFG copper samples and 1.0 μm for the CG copper samples. Orientation imaging microscopy (OIM) analysis software version 5.3 was used to analyze the orientation characteristics and the misorientation distribution. For the measurement of grain size, the specimens were mechanically polished to a thickness of 100 μm and then subject to twin-jet electropolishing using a solution comprising 200 mL of CH_3OH and 100 mL of HNO_3. The jet thinning was conducted at -30°C. Grain sizes were measured using a JEOL JME-2100F instrument at 200 kV.

The degree of non-equilibrium in the microstructure was measured using differential scanning calorimetry (DSC). The sample and reference were placed in thermally balanced alumina pans. The reference was made of the same copper as the sample but it was in the fully annealed state. All the experiments were performed using a nitrogen atmosphere in a DSC chamber with continuous heating and a ramp rate of 10°C/min up to 450°C.

3 Experimental results and discussion

Figure 1 represents the typical TEM micrographs and SADPs (selected area diffraction patterns) for ECAPed Cu processed by (a) 1, (b) 4, (c) 8 and (d) 12 passes. A large number of dislocation began to be observed in the specimen even after the 1st pass. After the 4th pass, equiaxed grains tended to form with an average size of 300 nm. The size of these grains did not vary with further ECAP process up to 12 passes. Once the equiaxed grains formed, the dislocation density inside the grain appeared to decrease with further ECAP process. To confirm this notion of the dislocation density reduction with the ECAP process, the heat flow

values of the specimens with different ECAP process cycles were measured by using DSC (Table 1). The rationale for this measurement is that the heat flow of pure copper would be solely controlled by the generation and/or annihilation of dislocations and grain boundaries (GBs) during ECAP processing, unlike the other alloys that either have had precipitation hardening or a solid solution-hardening mechanism. As might be expected, the heat flow values of the fully annealed copper were almost zero. With the ECAP process by one pass, the heat flow increased drastically accompanied with the increase in the dislocation density. Further the ECAP process, however, the stored energy, as represented by the heat flow value, began to gradually decrease reflecting the TEM observation shown in Figure 1. Therefore, we believed that the tensile strength values of pure Cu increased with the increasing number of ECAP passes due to the strain hardening in the initial stage. Further ECAP process promoted the formation of equiaxed grains accompanied with the gradual decrease in dislocation density. Once the equiaxed grain formed, the decrease in dislocation density would be further accelerated due to the extremely high rate of dynamic recovery with the GB area acting as a dislocation sink. The strain hardening mechanism would then stop to operate, or, at least, the role of the strain hardening mechanism would be weakened. Instead, the fine GB hardening mechanism would begin to dominate after the 4th pass of ECAP process. The mechanical properties and heat flow (HF) value of the specimens are summarized in Table 1.

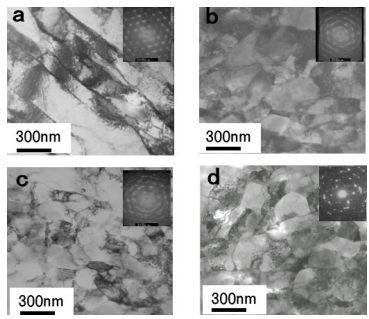

Figure 1: Typical TEM micrographs and the matching SADPs for ECAPed Cu processed by: a. 1, b. 4, c. 8, and d. 12 cycles.

Table 1: Mechanical properties and heat flow values.

Material	ECAP pass numbers	Yield strength (0.2%) YS MPa	Tensile strength *su* MPa	Total elongation *f*%	Heat flow J/g
CG	0	35	232	51.5	~ 0
UFG1	1	309	342	25.1	0.92
UFG2	2	376	399	23.2	—
UFG4	4	392	426	20.5	0.85
UFG8	8	414	435	22.6	0.69
UFG12	12	424	438	13.5	0.49

Figure 2 shows the YS, ultimate tensile strength (UTS) and tensile elongation (TE) values plotted as a function of the number of ECAP passes. Both YS and UTS values increased significantly in the initial stage (1 and 2 passes). After 2 passes, both values exhibited a gently increasing trend and tended to decrease in an increasing rate with the ECAP process from 8 to 12 passes. The TE dropped sharply after the first pass, followed by a temporary saturation trend during the 2nd to 8th passes. At the 12th pass, the TE dropped to about 60% of the 8 passes sample. Generally the plastic deformation depends on the generation and movement of dislocations. When the grain size is diminished to a submicron order, the cell-wall structures inside grains, which act as sources for dislocation, form with difficulty, leading to decreased ductility because of the suppressed generation of dislocations. Therefore, the microstructure of sample UFG12 with equiaxed-grains of submicron size exhibited reduced elongation. However, EBSD analysis ([11, 13] Figure 4(a)) showed that UFG4 and 8 had a heterogeneous structure with the presence of fine equiaxed grains and elongated large grains that contributed to a larger elongation than that of UFG12.

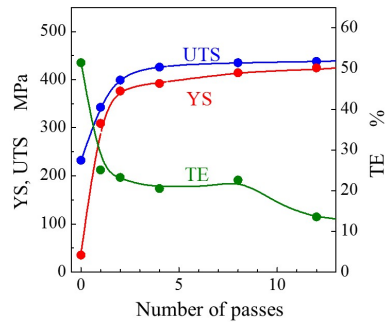

Figure 2: Tensile properties of UFG copper processed in the Bc route as a function of the number of ECAP passes.

Figure 3 shows S–N plots of data collected during stress-controlled fatigue tests. At high and medium stress amplitudes (σ_a > 100 MPa) a drastic enhancement of fatigue life occurred, which was attributed to grain refinement, e.g., the number of cycles to failure for UFG8 at σ_a = 130 MPa was about 15 times larger than that for annealed copper. However, the enhancement decreased with a decrease in stress amplitude; at low stress amplitudes corresponding to fatigue lifetimes above of 10^7 cycles, the S–N plots of all UFG copper samples tended to coincide with untreated conventional grain-sized copper. For the medium stress amplitudes corresponding to fatigue life from ~2×10^5 to 2×10^7 cycles, the difference in fatigue life with different pass numbers was clearly observed. Sample UFG12 presented the shortest life among the UFG samples. At high-stress amplitudes, however, the S–N plots tended to converge into one curve regardless of the number of passes. Regarding the fatigue strength of UFG copper at high-stress amplitudes corresponding to the LCF regime, it was shown [14] that the difference in purity was practically wiped off in S–N plots; nevertheless, the fatigue strength of high-purity copper at low-stress amplitudes was lower than that of low purity copper.

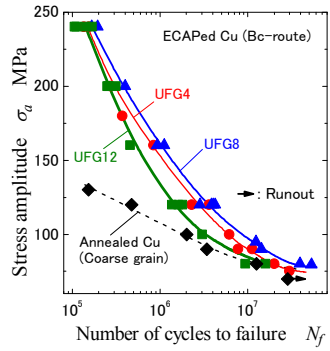

Figure 3: 3 S–N curves obtained under the stress controlled testing.

It has been shown that the grain coarsening as a result of cyclic stressing occurs in UFG copper processed by SPD technique [5, 8, 9]. Figure 4 shows inverse pole figure (IPF) maps and GB maps of (a) a post-ECAP UFG8-sample (pre-fatigue), (b) and (c) samples fatigued with a constant stress of σa = 240 and 90 MPa . The maps for fatigued samples were taken from regions adjacent to crack paths.

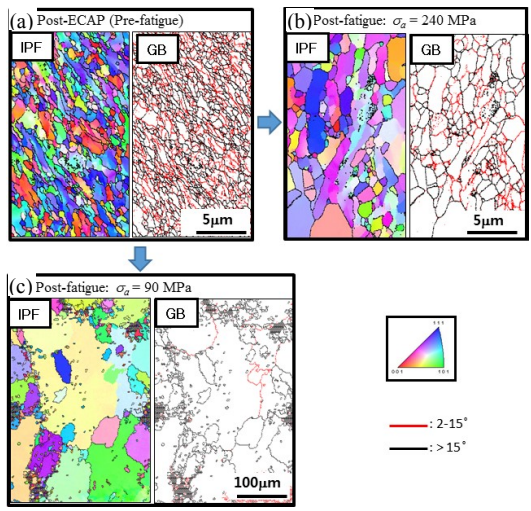

Figure 4: OIM orientation and GB maps for sub-surface microstructures in UFG8: (a) original microstructure before stressing; (b) after constant stressing at σ_a = 240 MPa; (c) after constant stressing at σ_a = 90 MPa.

The GBs in GB maps are denoted either by red lines corresponding to low-angle GBs (LAGBs), where the misorientation, θ, is between 2° and 15°, or by black lines corresponding to high-angle GBs (HAGBs) with $\theta > 15°$. The IPF and GB maps of post-ECAP copper (Figure 4(a)) exhibit inhomogeneous microstructures that include fine equiaxed grains and large elongated grains. These maps indicate

the development of subgrains within elongated grains, isolated with LAGBs. Thus, the microstructure in post-ECAP copper has enhanced strain energy due to the redundant defect structure, and the microstructure is therefore in the process of evolving to equiaxed grains isolated with HAGBs. The post-fatigue microstructure subjected to the constant stressing experienced grain coarsening, but the coarse grain sizes depended on the applied stress amplitudes. At high stress amplitude of σ_a= 240 MPa, coarse grains evolved from 1 to 10 μm (Figure 4(b)). At a low stress amplitude of σ_a= 90 MPa , long-term repetitions produced large coarse grains in excess of several tens of micrometers (Figure 4(c)).

Figure 5 shows the change in surface states due to constant stressing of σ_a = 90 MPa for (a) UFG4, (b) UFG8 and (c) UFG12. Prior to taking OM micrographs of damaged surfaces, the specimen surfaces were etched to reveal the microstructure after polishing off a few micrometers from the surface layers of the fatigued specimens. For UFG4 (Fig. 5(a)), blurry bright areas appeared at $N = 1.6 \times 10^7$ cycles. However, clear bright areas appeared at $N = 6 \times 10^6$ cycles for UFG8 and $N = 4 \times 10^6$ cycles for UFG12. These areas indicate coarse grains as a result of dynamic recrystallization. The coarse grains gradually grew with subsequent stressing, and their size exceeded 200 μm with further stressing. The large coarse grains were not necessarily formed by the growth of a single grain, but by clusters of several larger grains which grew individually until GBs reached neighboring grains. The number of cycles required to form recrystallized grains tended to be smaller in UFG12 than UFG4 and 8.

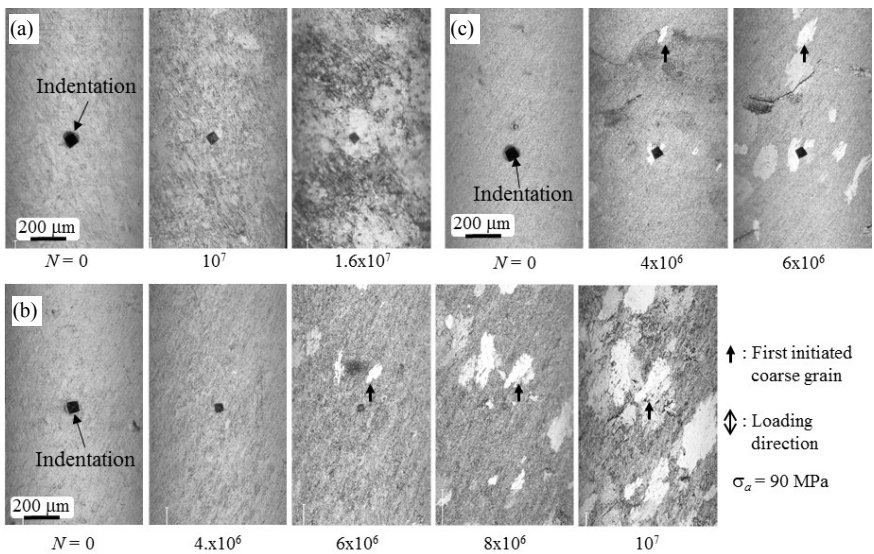

Figure 5: Change in surface states due to cyclic stressing at σ_a = 90 MPa revealed by etching; (a) UFG4, (b) UFG8 and (c) UFG12. For easy recognition of the location where grain growth occurred, an indentation was added at an arbitrary site on each prefatigued surface.

The initiation life of fatigue cracks should affect the fatigue life of the specimens. In addition, strain localization due to slip band formation are likely to lead to the crack initiation. Figure 6 shows the SEM micrographs of surface states around typical fatigue crack imitation sites for UFG4, showing a crack initiated within slip bands and a crack initiated at the boundaries of coarsened grains with slip bands.

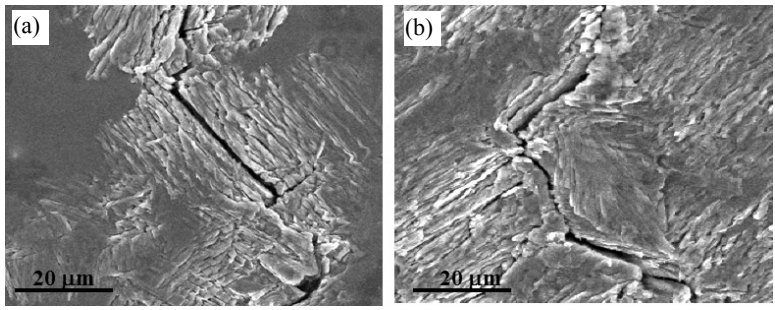

Figure 6: SEM micrographs of surface states around typical fatigue crack imitation sites for UFG4 (σ_a = 120 MPa): (a) crack initiated from slip bands in coarse grains; (b) crack initiated at the boundaries of coarsened grains with slip bands.

To elucidate the role of grain coarsening on the slip-band/crack formation, the changes in surface states due to cyclic stressing (σ_a = 120 MPa) were monitored in four areas (1.7×0.8 mm^2 × 4) set on the mid-surface of specimens. Figure 7 shows the change in surface states around the first formed damaged areas in the wholly monitored areas. The first slip bands of UFG12 were observed at 2.5×10^5 cycles. For UFG4 and 8, however, the first slip bands were recognized at 7.5×10^5 cycles. Regarding the formation pattern of the damaged areas, the pattern for UFG8 and 12 was distinguishable from that for UFG4. For UFG8 and 12, damaged areas formed at an early fatigue stage extended their sizes only with subsequent stressing. In other words, oriented slip bands inside the areas increased their length and number with cyclic stressing. For UFG4, damaged areas in close proximity were formed simultaneously. With further stressing, other damaged areas were incidentally generated in close proximity to the initial damaged areas after their slight extension, bringing the extension of damaged areas as an aggregate.

Figure 8 presents the SEM micrographs of the damaged areas shown in Figure 7. From the aspect of the slip bands seen in the SEM images for UFG8 and 12 (Figure 8(b), (c)), slip bands inside the island-like damaged areas had the same orientation as indicated by double-head arrows, suggesting the slip bands of single recrystallized grains. However, damaged areas for UFG4 (Fig. 8(a)) consisted of slip bands formed in some adjacent grains with an individual crystallographic slip orientation.

Nuclei of dynamically recrystallized grains may be easy to generate in microstructure with a large fraction of HAGBs having high strain energy, such as

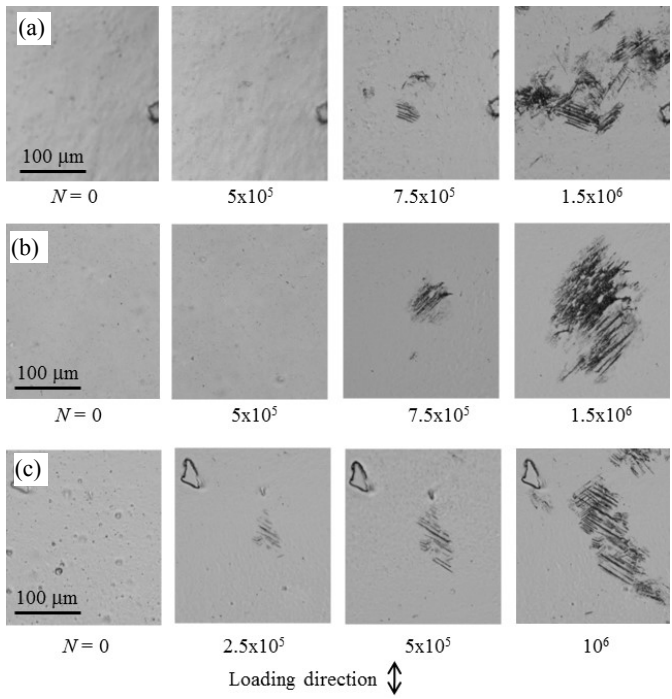

Figure 7: Extension behavior of the first initiated slip bands in monitored areas during stressing of σ_a = 120 MPa: (a) UFG4; (b) UFG8; (c) UFG12.

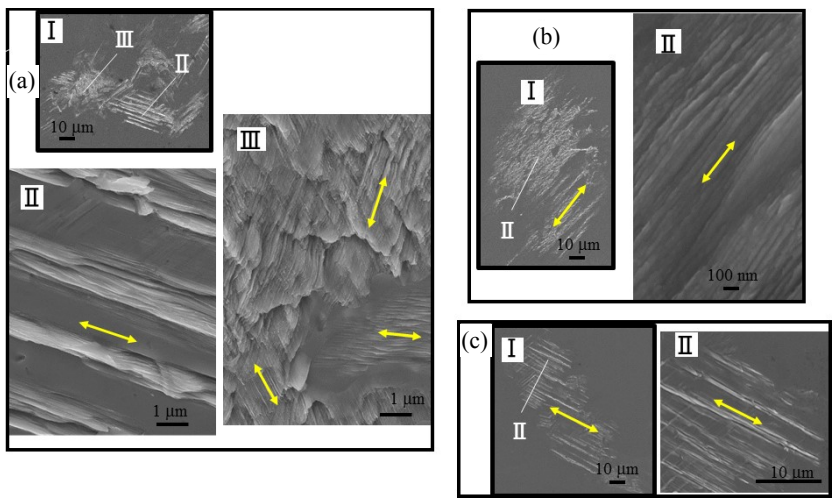

Figure 8: SEM micrographs of damaged areas in Figure 7: (a) UFG4; (b) UFG8; (c) UFG12, a double-head arrow shows the slip orientation.

UFG12. After the nucleation, the recrystallized grains continued to grow with cyclic stressing, followed by slip band formation inside evolved grains with a favorable slip orientation and size. Subsequent stressing brought a further increase in both grain size and number/length of slip bands. On the other hand, for UFG4, the formation of slip bands was likely to occur during the progress of the dynamic recovery process, meaning a limited involvement of the dynamic recrystallization on the formation of coarse grains at the initial stage of fatigue lifetime. Because the UFG4 microstructure had a high fraction of LAGBs and large elongated grain/cell structures with a high population of defects (dislocations/sub-GBs), coarse grains could form by annihilation of such defects inside or at boundaries of the original large elongated grains as a result of dynamic recovery, followed by slip band generation inside the coarse grains. With further cyclic stressing, the damaged areas became visible as the aggregates of recovered coarse grains with their specific slip orientations.

Although the collective damaged areas (composed of some nearby damaged areas) in UFG4 were much larger than the largest damaged areas in UFG12, the size of damaged areas distinguished by a single slip orientation was larger in UFG12 than in UFG4 (Figure 8), indicating a lower resistance to crack initiation in UFG12. Accordingly, the shorter fatigue life of UFG12 at medium and low stress amplitudes resulted from diminished crack initiation life because of accelerated slip band formation caused by early formation of large recrystallized grains. It has been shown that the difference in pass number in UFG copper has a negligible effect on the crack growth rate [15]. Here, one should be aware that the occurrence of the dynamically recovered grains in UFG4 never imply no generation of dynamically recrystallized grains. Dynamically recrystallized grains larger than 100 μm, which tended to form in the later stages of fatigue, were detected on the surface of postfatigued UFG4 specimens. The grain growth was notable at lower stress amplitudes with a large number of stress cycles to failure. Such a dynamic grain growth to a grain size of over 100 μm during cyclic deformation would accelerate the fatigue damage accumulation process and drastically decrease the resistance to fatigue at a low applied stress range corresponding to fatigue lifetimes in excess of 10^7 cycles.

4 Summary

The main findings of this study can be summarized as follows: The UFG4 samples exhibited inhomogeneous microstructures including fine equiaxed grains and large elongated grains. The microstructure of UFG8 was composed of fine equiaxed grains and elongated large grains like UFG4, but both the fraction and size of the elongated grains were smaller than those of UFG4. On the other hand, the microstructure of UFG12 samples retained a large fraction of equiaxed grains with HAGBs. For UFG8 and 12, dynamically recrystallized grains were formed and these grew with subsequent stressing upon slip-band formation. Slip bands were initiated inside such grains. With further stressing, the coarse grains continued to grow and both the number and length of slip bands inside the grains increased with grain growth. For UFG4, the formation of slip bands was

likely to occur during dynamic recovery. Because the UFG4 microstructure had a high fraction of LAGBs and large elongated grains/cells with a high defect population, coarse grains were produced by annihilation of such defects inside or at the boundaries of the original large, elongated grains as a result of dynamic recovery. Slip bands were formed inside such coarse recovered grains.

Acknowledgements

This study was supported by a Grant-in-Aid for Scientific Research (C) (KAKENHI: No. 26420021) from the Japan Society for the Promotion of Science (JSPS), as well as a National Research Foundation of Korea (NRF) grant funded by the Korean Government (MSIP) (No. 2011-0030058), and by a grant from the Global Frontier R&D Program (2013M3A6B1078874) on Global Frontier Hybrid Interface Materials R&D Center funded by the Ministry of Science, ICT and Future Planning. The authors are very grateful to the members of the Strength of Materials Laboratory of Oita University for their excellent experimental assistance. Thanks are also extended to the members of the Korea Institute of Materials Science, for performing the ECAP processing of our copper rods.

References

[1] Segal, V.M., Materials processing by simple shear. *Materials Science and Engineering,* **A197**, pp. 157–164, 1995.
[2] Agnew, S.R., & Weertman, J.R., *Materials Science and Engineering*, **A244**, pp. 145–153, 1998.
[3] Vinogradov, A. & Hashimoto, S., *Materials Transactions*, **42**, pp. 74–84, 2001.
[4] Höppel, H.W., Zhou, Z.M., Mughrabi, H. & Valiev, R.Z., *Philosophical Magazine*, **A 87**, pp. 1781–1794, 2002.
[5] Mughrabi, H., Höppel, H.W. & Kautz, M., *Scripta Materialia*, **51**, pp. 807–812, 2004.
[6] Vinogradov, A., Nagasaki, S., Patlan, V., Kitagawa, K. & Kawazoe, M., *NanoStructure Materials*, **11**, pp. 925–934, 1999.
[7] Goto, M., Han, S.Z., Yakushiji, T., Lim, C.Y., & Kim, S.S., *Scripta Materialia*, **54**, pp. 2101–2106, 2006.
[8] Khatibi G, Horky J, Weiss B, & Zehetbauer M.J., *International Journal of Fatigue*, **32**: pp. 269–278, 2010.
[9] Han S.Z., Goto M., Ahn J.H, Lim S.H, Kim S., & Lee J. *Journal of Alloys and Compounds,* **615**: S587–589, 2014.
[10] Kunz L, & Lukáš P, & Svoboda M. *Materials Science and Engineering,* **A434**, pp. 97–104, 2006.
[11] Goto M, Han SZ, Ahn JH, Yakushiji T, Euh K, Kim SS, & Lee J. *International Journal of Fatigue*, **66**, pp. 220–228, 2014.
[12] Iwahashi Y, Wang J, Horita Z, Nemoto M, & Langdon T.G., *Scripta Materialia*, **35**: pp. 143–146, 1996.

[13] Goto, M., Han, S.Z., Euh, K., Kang, J-H., Kim, S.S., & Kawagoishi, N., *Acta Materiala*, **58**, pp. 6294–6305, 2010.
[14] Lukáš P., Kunz L., & Svoboda M., *Kovove Materials*, **47**: pp. 1–9, 2009.
[15] Goto, M., Han, S.Z., Ando, Y., Kawagoishi, N., Teshima, N., & Kim, S.S., *WIT transaction on Modelling and Simulation*, **48**, pp. 497–508, 2009.